Rational Sidewall Functionalization and Purification of Single-Walled Carbon Nanotubes by Solution-Phase Ozonolysis

Sarbajit Banerjee[†] and Stanislaus S. Wong*[,†,‡]

Department of Chemistry, State University of New York at Stony Brook, Stony Brook, New York 11794, and Materials and Chemical Sciences Department, Brookhaven National Laboratory, Building 480, Upton, New York 11973

Received: June 13, 2002; In Final Form: October 2, 2002

A dispersion of raw HiPco single-walled carbon nanotubes in methanol has been subjected to ozonolysis at −78 °C, followed by treatment with various reagents, in independent runs, to generate a higher proportion of carboxylic acid/ester, ketone/aldhehyde, and alcohol groups, respectively, on the nanotube surface. This protocol has been found to purify nanotubes by removing amorphous carbon and metal impurities. More importantly, as had been theoretically predicted, the reaction sequence has been found to ozonize (and hence, oxygenate) the sidewalls of these nanotubes, thereby broadening the chemical processability and reactivity of these nanomaterials. The derivatized materials have been characterized by means of SEM and TEM, and spectroscopically, using Raman, UV−vis−near-IR, and X-ray photoelectron spectroscopies.

Introduction

Single-walled carbon nanotubes (SWNTs) are important for a number of nanotechnology applications,[1] due to their favorable, structure-dependent mechanical[2] and electronic[3] properties. The problem with the synthesis of SWNTs, though, is that the as-prepared material frequently contains a number of metallic and amorphous impurities, interfering with their reliable and optimal usage in applications such as field emission displays, molecular computers, and ultrahigh strength materials. While published techniques based on bromination,[4] plasma etching,[5] chromatographic separation,[6,7] cascade membrane microfiltration,[8] and sonication[9] of nanotubes in surfactant exist to rid SWNTs of such impurities, more common purification methods of SWNTs involve a combination of oxidative processes, such as acid reflux in solution or gaseous oxidation, to obtain high-quality tubes.[10−13]

In effect, these oxidative processes are capable of generating a variety of oxygenated functional groups, such as aldehydic, ketonic, esteric, alcoholic, and carboxylic moieties,[14,15] at the nanotube ends and in particular, at structural defect sites along the tube walls, etched by the oxidizing agent. In particular, the assumed predominance of carboxylic acid groups, after these strong oxidative procedures, has been the basis for much of the interesting chemistry that has been reported with SWNTs, thus far. Notably, oxidized SWNTs have been solubilized by reaction with long-chain amines,[16] by mixing with polymers,[17] and through coordinate complexation using metal complexes.[18,19] Recently, titanium oxide nanocrystals and quantum dots have also been attached to oxidized SWNTs using carbodiimide chemistry which has taken advantage of the presence of these oxygenated groups.[20]

What has not been readily determined in these systems, though, is the number, distribution, and location of these generated oxygenated functional groups. Addressing this issue will aid in achieving rational spatial and molecular control over chemical derivatization in nanostructures. This ability to demonstrate controlled chemistry not only has relevance for photophysical analyses of SWNTs but also for rational modulation of their electronic and mechanical properties. Indeed, this study, in particular, through the chemical modification of sidewalls, has implications for lithium intercalation[21] and adsorption and storage of gases,[22] as well as other types of molecular species, onto and within nanotubes.[23,24]

Herein, we describe a "one-pot" oxidative methodology with three major objectives: first, the purification of as-prepared SWNTs to obtain a high-quality product; second, the chemical functionalization of nanotube sidewalls; and third, a systematic procedure to rationally skew the distribution of oxygenated functional groups to favor (i.e., generate higher proportions of) one particular moiety, through a reproducible chemical protocol, on the surfaces of the resultant purified SWNTs. These goals are accomplished by favoring the generation of carboxylic acids, aldehydes/ketones, and alcohols on the surfaces of carbon nanotubes through chemical treatment with hydrogen peroxide (H_2O_2), dimethyl sulfide (DMS), and sodium borohydride ($NaBH_4$), respectively, that take advantage of the high reactivity of primary ozonides, that are presumed to form upon the ozonolysis of SWNT dispersions in solution.

Why ozonolysis? Ozone (O_3) has been described as a good oxidizing agent for the purification of nanotubes.[11] Moreover, O_3 is predicted[25] to add to the double bonds of SWNTs in an analogous way to that of alkenes and fullerenes,[26] through a facile 1,3-dipolar cycloaddition reaction following Criegee's mechanism. The expected primary ozonide thereby formed is rather unstable and may readily dissociate, as is the case with fullerenes.[27] In the presence of a variety of carefully chosen oxidizing and reducing agents, the ozonide can be cleaved to yield a wide distribution of functional groups in a more predictable manner.

Whereas previous ozonolysis reactions with SWNTs have been reported to occur at the end caps,[28] as we will show, this

* To whom correspondence should be addressed. Telephone: 631-632-1703; 631-344-3178. E-mail: sswong@ms.cc.sunysb.edu; sswong@bnl.gov.
† State University of New York at Stony Brook.
‡ Brookhaven National Laboratory.

10.1021/jp026304k CCC: $22.00
Published on Web 11/01/2002

work represents the first instance of sidewall functionalization of SWNTs with oxygenated functionalities. The implication, then, is the generalization of previously reported nanotube chemistry, commonly localized at the ends of tubes and at a few isolated defects, which can henceforth be replicated in a controllable manner along the sidewalls and lengths of these tubes. In addition, this provides experimental verification[25] for the use of ozonolysis as a means of rationally derivatizing SWNT sidewalls.

Thus, not only is a certain degree of spatial control of chemical derivatization of SWNTs achievable but also these experiments can be performed with nanotubes in the solution phase, which avoids the potentially damaging consequences of ozonolysis at high temperatures in the gaseous phase. Our solution phase ozonolysis protocol is milder, operates at low temperatures, and, coupled with the cleavage reaction and subsequent workup, can further enhance the intrinsic purity of the resultant SWNT material with minimal sample loss. Overall, these purification conditions maximize SWNT yield, which is particularly important for samples, such as the commonly used HiPco tubes.[29]

The purity of the SWNT material and the resultant distribution of the oxygenated functional groups have been structurally characterized by X-ray photoelectron spectroscopy (XPS), scanning electron microscopy (SEM), and transmission electron microscopy (TEM). Optical information, confirming sidewall functionalization, has been collected using UV−visible, near-infrared (NIR), and Raman spectroscopies.

Experimental Section

Ozonolysis of SWNTs. The ozonolysis reaction was carried out on a commercial Welsbach ozonolysis apparatus. In this instrument, the flow of O_2 to the arc discharge is kept below 1.5 psi. Ozone is formed in a 185 W discharge with the pressure adjusted to maintain a constant flow of a ~10% O_3 in oxygen mixture to the sample at a pressure of under 3 psi. Typically, 100 mg of as-prepared HiPco SWNTs (Carbon Nanotechnologies, Houston, TX) were first dispersed in 150 mL methanol (MeOH) by extensive sonication, prior to each 1 h run. The reaction mixture was stirred vigorously during ozonolysis, which was carried out at −78°C by placing the reaction flask in a dry ice/acetone bath, to create the expected ozonide intermediate. The reaction mixture was then flushed with O_2 at the end of ozonolysis to rid the solution of any remaining O_3.

Controllable Modification of Ozone-Treated Tubes. The expected primary ozonide generated can be cleaved in a number of ways by initial incubation with specific reagents at −78 °C. The "cleaving" agents used included H_2O_2, DMS, and $NaBH_4$, yielding samples designated **1**, **2**, and **3**, respectively.

In the case of sample **1**, upon addition of ~10 mL of 50% H_2O_2 in aqueous solution, the sample was heated to 70 °C and refluxed for 4 h. The H_2O_2-cleaved tubes were then filtered over a 0.2 μm polycarbonate membrane and washed with a large excess of MeOH to remove any lingering H_2O_2 as well as any impurities such as amorphous carbon.

To create samples **2** and **3** respectively, DMS and $NaBH_4$ were added in large excess. After the reaction was stirred for 24 h, the DMS-cleaved tubes were filtered over 0.2 μm polycarbonate membranes; the residue was washed extensively with methanol to quench the DMS. With the $NaBH_4$-cleaved tubes, after the reaction was stirred for 12 h, the borohydride reagent was quenched by addition of 12.1 N HCl. The resultant tubes were filtered over a 0.2 μm polycarbonate membrane and then washed continuously with concentrated HCl and with methanol. All samples, **1** through **3,** were washed with copious amounts of distilled, deionized water.

A control sample, **Ctrl**, was generated by subjecting a nanotube sample to ozonolysis in methanol but without the addition of any further "cleaving" reagent. To reflect the types of treatment of the other samples, the control was filtered over a 0.2 μm polycarbonate membrane and washed extensively with methanol and H_2O.

As a final step, the samples, which resembled mats of bucky paper, were peeled off from the filter membranes and dried in a heating oven at 100 °C.

X-ray Photoelectron Spectroscopy. For XPS analysis, the solid samples were attached to stainless steel holders using conductive double-sided tape and installed in the vacuum chamber of a XPS surface analysis system (Kratos Analytical Plc model DS800). The chamber was evacuated to a base pressure of about 5×10^{-9} Torr. A hemispherical energy analyzer was used for electron detection. XPS spectra were first collected using a Mg Kα X-ray source at 80 eV pass energy and at 0.75 eV steps for each sample. High-resolution spectra were collected at a pass energy of 10 eV and in 0.1 eV steps.

Electron Microscopy. Samples for TEM were obtained by drying sample droplets from an ethanolic solution onto a 300 mesh Cu grid with a lacey carbon film. All the micrographs were taken at an accelerating voltage of 120 kV on a Philips CM12 TEM, equipped with EDAX capabilities. Samples for SEM were drop dried on Cu grids and imaged in a homemade sample holder on a Leo 1550 field emission instrument at accelerating voltages ranging from 2 to 10 kV at a 2 mm working distance.

Optical Spectroscopy. UV spectra were obtained at high resolution on a ThermoSpectronics UV1 using quartz cells with a 10 mm path length. Near-IR spectra were obtained in transmission on a Vector 33 spectrophotometer (Brüker Optics), after 32 scans, using a 1 mm path length capillary tube. UV−vis and near-IR spectra were obtained by dissolving the SWNT samples in *o*-dichlorobenzene (ODCB) by sonication and were corrected to account for the solvent background. FT Raman spectra were collected on a RFS 100 spectrometer by placing the samples on an aluminum slide and collecting data in a standard macrochamber. The Raman data were obtained, after 256 scans, upon excitation of a 1064 nm Nd:YAG laser at a power of ~100 mW, using a liquid N_2 cooled Ge detector.

Results and Discussion

I. Purification. Previous studies of ozonolysis of nanotubes in solution simply mention that the tubes have been opened and, unfortunately, address neither purification nor the presence and location of functional groups.[26] In this study, the SEM (Figure 1) and TEM (Figure 2) micrographs indicate the increased purity of the ozonized tubes, compared with as-prepared tubes. For instance, a large amount of contaminant material, particularly amorphous carbon, noted in Figure 1a, in the initial, raw HiPco sample, is substantially removed in the subsequent micrographs (Figure 1, parts b−e) after ozonolysis and associated treatments. This is not altogether surprising.

It is reasonable, for instance, to expect that, upon ozonolysis, amorphous carbon detritus, onions, and nanoparticles will become heavily functionalized with oxygenated groups and thereby have increased solubility in polar solvents, used to wash these samples. The reactivity of these contaminant materials is analogous to the reactivity at the end caps of the tubes, which are opened upon oxidation.[26,30,31] Indeed, there is also enhanced reactivity in regions of increased curvature and conformational

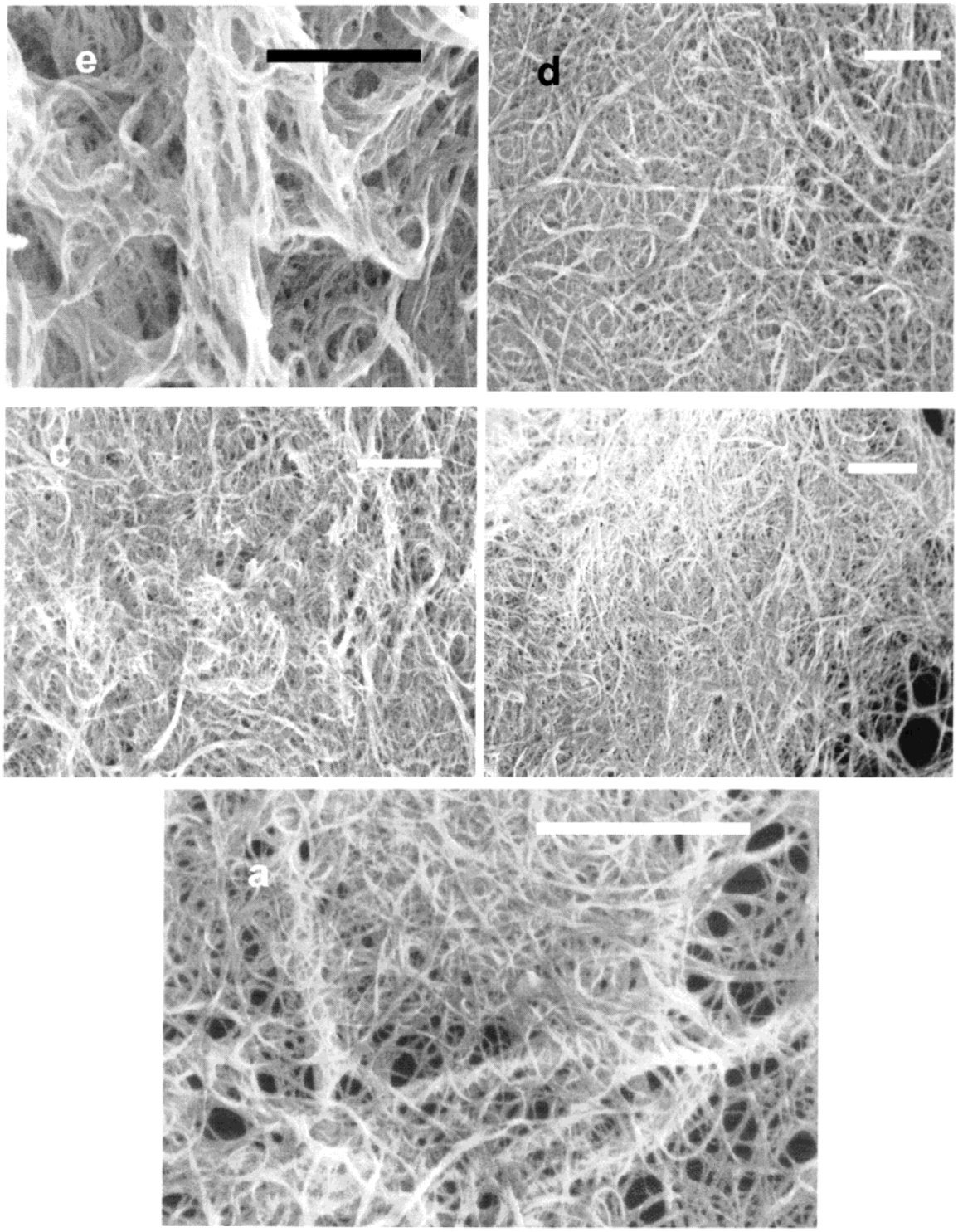

Figure 1. Scanning electron micrographs of a number of SWNT samples: (a) sample **1** (with H_2O_2); (b) sample **2** (with DMS); (c) sample **3** (with $NaBH_4$); (d) **Ctrl** ozonized sample; (e) raw, as-prepared HiPco. Scale bars for these micrographs are 1 μm in each case.

strain, notably at high densities of pentagonal and heptagonal defect sites.[31,32] Ozone can oxidize[10,13] the graphitic coating surrounding the Fe metal catalyst particles to their corresponding, less dense iron oxides, which can then breach the carbon shells, exposing metal particulates to further removal by chemical reagents. As such, the ozonolysis process essentially facilitates the elimination of the unwanted Fe metal by subsequent chemical processing of SWNTs during sidewall functionalization.

For example, hydrogen peroxide can leach iron oxide clusters into solution.[33] Thus, the O_3/H_2O_2 combined protocol should be very successful at removing iron, which is evident as seen in sample **1**, shown in Figure 1e, to a percentage of about 0.25% from a high of about 4−5% in unprocessed HiPco. Use of hydrogen peroxide alone, without ozonolysis treatment, is able to reduce the iron content to 1.37%, indicating the ability of this reagent to leach iron oxide clusters into solution. After ozonolysis, the processing of sample **3** involves an acid treatment to quench the borohydride reagent, which has the complementary effect of lowering Fe concentrations to only 0.48%. It is of note that a $NaBH_4$/HCl treatment, without ozonolysis, on the SWNTs can reduce the iron content in the

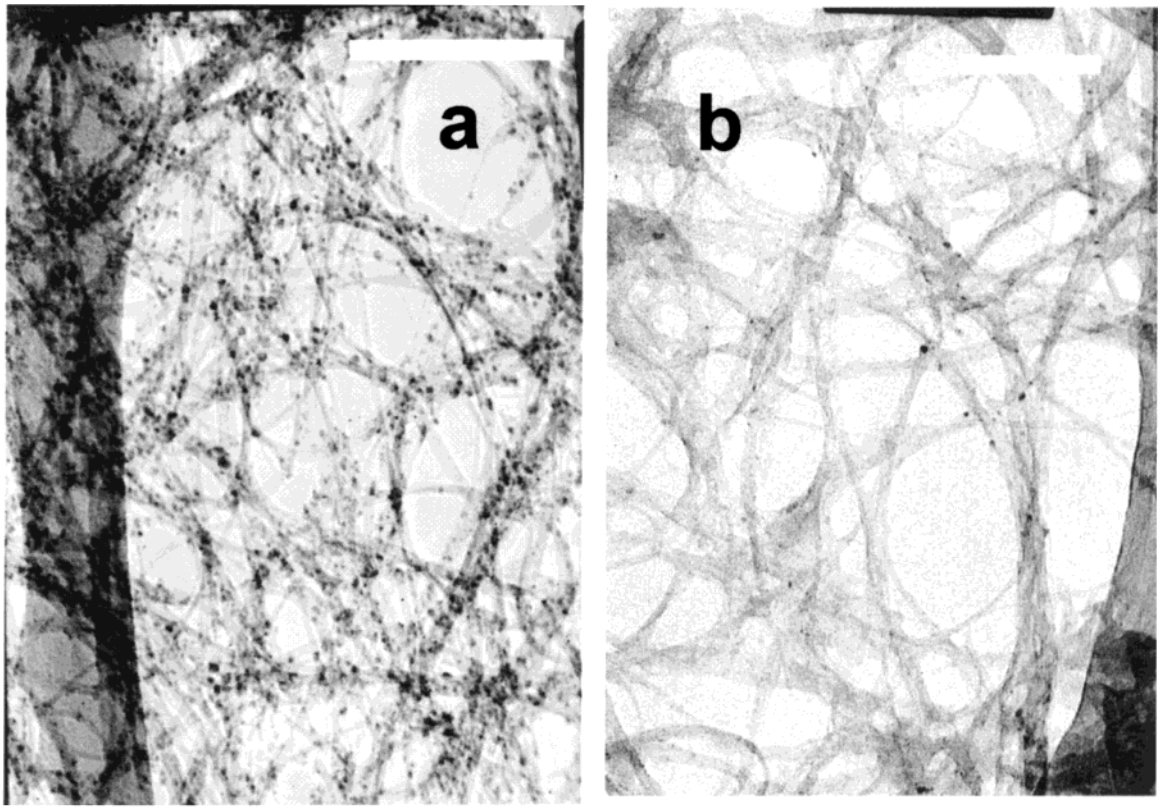

Figure 2. Transmission electron micrographs of (a) as-prepared HiPco SWNTs and (b) SWNTs after ozonolysis and HCl treatment. Scale bars are 130 and 140 nm, respectively.

sample to ∼1.16% only. The implication then is that most of the residual, extraneous iron is likely encapsulated within a carbon shell, that needs to be reacted with ozonolysis, in order for it to be properly eliminated by means of HCl. Indeed, use of DMS or $NaBH_4$ alone is not expected to be capable of removing Fe but rather is a means of obtaining some level of rational chemical control over the identity of the resultant functional groups on the tube surface. Thus, ozonolysis, coupled with further specific chemical processing, appears to be best suited for SWNT purification.

In effect, the ozonized, purified nanotubes form close-packed, ordered bundles, which, compared with as-prepared HiPco tubes, are more difficult to disperse and solubilize in nonpolar, organic solvents, such as ODCB. This is likely an effect not only of the increased crystallinity of these tubes but also of the abundance of polar groups present on the SWNT surface, leading to the likelihood of increased hydrogen bonding interactions that can result in better packing and stacking among the tubes within the bundles.[34] Sample **1**, for instance, could be easily dispersed in dimethyl sulfoxide (DMSO).

II. Sidewall Functionalization. Raman spectra for HiPco tubes and for samples **1**−**3** as well as the **Ctrl** sample are shown in Figure 3. Raman spectroscopy is particularly important for understanding the vibrational and electronic properties of nanotubes and fullerenes. For instance, whereas the radial breathing modes (RBM)[35,36] near 200 cm^{-1} depend sensitively on tube diameter, the high-frequency tangential displacement G modes[37] near ∼1590 cm^{-1} and the second-order G′ bands[38] near 2600 cm^{-1} are sensitive to the charge exchanged between nanotubes and guest atoms that have intercalated into the interstitial channels in the tube bundles. Importantly for this work, the shape and intensity of a weak disorder mode peak at 1290−1320 cm^{-1} has been correlated with the extent of nanotube sidewall functionalization.[39] Other bands occur in the

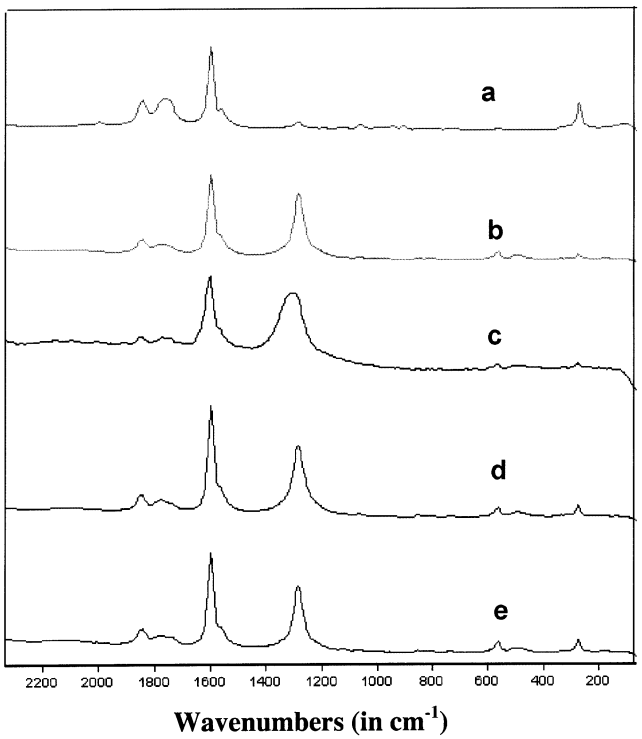

Figure 3. FT-Raman spectra of (a) as-prepared HiPco, (b) sample **2** (with DMS), (c) sample **1** (with H_2O_2), (d) **Ctrl** sample, and (e) sample **3** (with $NaBH_4$). Upon ozonolysis, the intensity of the D line is greatly increased relative to that of the G line. The Raman spectra were obtained on solid samples, placed on Al slides.

1600−1900 cm^{-1} region of the Raman spectra. The origin of these peaks is not due to impurities but rather to second-order features arising from combination modes.[40,41] Specifically they correspond to $\omega_{tangential} + \omega_{RBM}$ and $\omega_{tangential} + 2\omega_{RBM}$

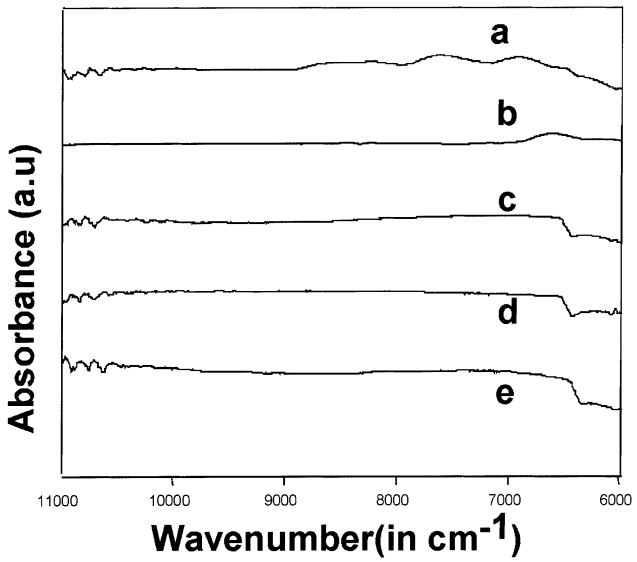

Figure 4. Near-IR spectra of (a) as-prepared HiPco, (b) sample **1** (with H_2O_2), (c) sample **2** (with DMS), (d) sample **3** (with $NaBH_4$), and (e) **Ctrl** sample. All the samples were in ODCB solution. The spectra were background subtracted for the solvent.

combination bands.[40] Because of resonant Raman effects linked to singularities in the one-dimensional electron density of states in the first-order spectra, these phenomena also give rise to resonant effects in the associated combination modes. It is of note that the laser excitation at 1064 nm used will probe primarily semiconducting tubes.[42,43]

A recent theoretical study[25] suggested that ozonolysis of nanotube sidewalls is facile. The Raman spectra for these samples are indicative that substantial sidewall functionalization does indeed take place while still preserving the tubular nature. Primary evidence for sidewall functionalization comes from the increased intensity of the disordered sp^3-hybridized D line at $\sim$1320 cm^{-1} with respect to the tangential nanotube Raman mode near 1590 cm^{-1}. The increased ratio of the disorder band intensity to the tangential mode intensity is widely accepted as arising from sidewall functionalization, due to the increased numbers of sp^3-hybridized carbon atoms in the hexagonal framework of the SWNT sidewalls.[44−46] The chemical derivatization effectively perturbs the excitations between π-bands of the bare sp^2-hybridized HiPco tubes. Because of the weakness of the disorder band in raw HiPco tubes, the high purity of the functionalized samples, as evidenced by the microscopy data, precludes amorphous carbon, detritus, and nanobubbles as being the origin of the disorder band noted with the processed samples.

To the extent that ozonolysis likely increases the presence of defect sites on the tube surface, it is highly unlikely that the reaction would seriously etch and physically destroy the SWNTs themselves, as would be apparent from acid treatments,[47] which would cut the ends of these tubes into smaller fragments, for instance. That is, based on the SEM micrographs, no real shortening of the tubes was observed, prior to and after ozonolysis, and hence, a simple increase of defect sites at the ends and sidewalls of these SWNTs, due to ozonolysis "damage" is unlikely to be a significant contributor to the increase in the intensity of the disorder peak observed. Hence, the presence of sidewall functionalization, and the accompanying perturbation of electronic structure, effectively is responsible for the increase in the disordered D line.

Moreover, a decrease[48] in the intensity of the RBM bands upon ozonolysis also is suggestive of the formation of covalent bonds along the sidewalls. The decrease of intensity of the second-order peaks observed with functionalization follows the trend of the first-order RBM peaks and is expected from the perturbation of the electronic density of states of SWNTs, which is evidenced by the absence of the optical transitions between the van Hove singularities. More specifically, the decrease in intensity likely originates in disruption of electron−phonon coupling interactions, unique to the one-dimensional structure of electronic states for SWNTs. These results provide for additional confirmation of sidewall functionalization.

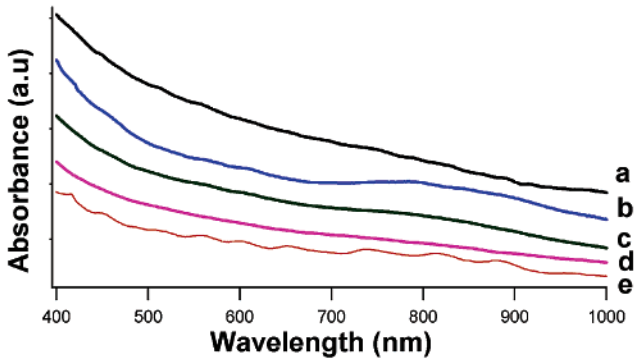

Figure 5. UV−vis spectra in ODCB of (a) sample **1** (with H_2O_2) (black), (b) sample **2** (with DMS) (blue), (c) sample **3** (with $NaBH_4$) (green), (d) **Ctrl** sample (pink), and (e) as-prepared HiPco (red). The individual spectra are offset for clarity.

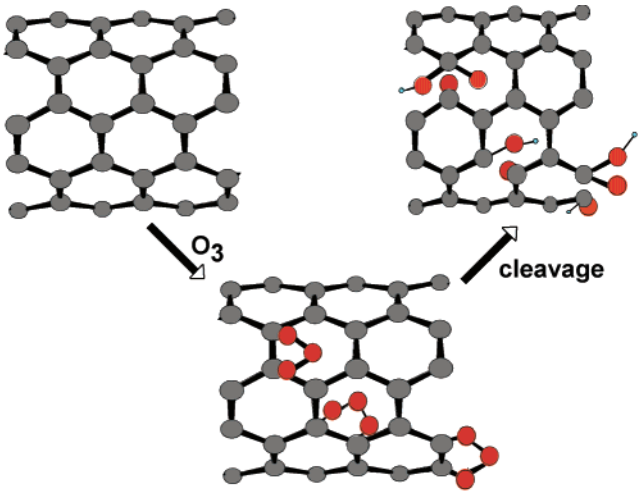

Figure 6. Schematic of a section of a SWNT sidewall. Upon treatment with ozone, a proposed intermediate, a primary ozonide, forms. Cleavage of the ozonide with selected chemical agents can yield a range of different functional groups. As examples, the presences of aldehydic, ketonic, alcoholic, and carboxylic groups are schematically illustrated.

Further evidence for sidewall functionalization comes from near-IR (Figure 4) and UV−visible spectra (Figure 5). The features seen in the UV−vis−NIR spectra of pristine SWNTs arise from optical transitions between van Hove singularities of the local electronic density of states of these tubes.[39,49] Sidewall functionalization is predicted to disrupt the electronic structure of SWNTs and, hence, cause a loss of these features,[44,45] whereas oxidative purification has been shown to perturb their intensity.[10,13] Indeed in the UV−visible spectra, distinctive peaks[50] corresponding to the second transition of semiconducting SWNTs (550−900 nm) and the first transition of metallic tubes (400−600 nm) are noted for the HiPco tubes dispersed in ODCB. After the ozonolysis reaction, these features are substantially broadened and are diminished in resolution. Similarly, in the NIR spectra, HiPco tubes show low energy features,[50] corresponding to the first band gap transition (6000−7500 cm^{-1}) of semiconducting tubes. In an analogous fashion,

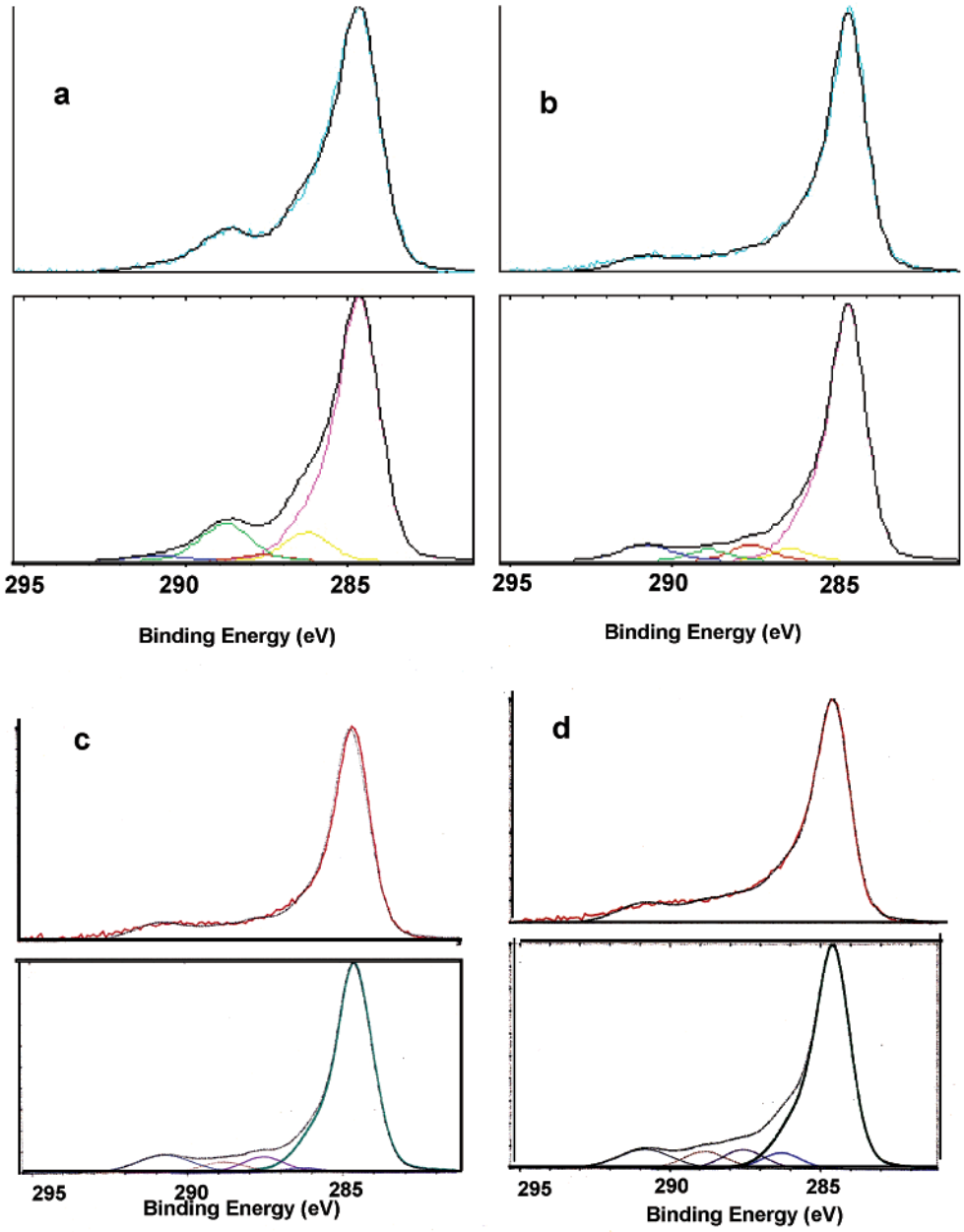

Figure 7. Pairs of high-resolution C_{1s} XPS spectra for (a) sample **1** (with H_2O_2), (b) sample **2** (with DMS), (c) sample **3** (with $NaBH_4$), and (d) **Ctrl** sample. The bottom half of each figure pair in each section shows the curve fittings to the C_{1s} peak. The spectra are fitted to nanotube carbons at 284.6 eV and to C−O, C═O, and O−C═O functional moieties at 286.3, 287.6, and 288.8 eV, respectively.

after the ozonolysis reaction, the resultant spectra are featureless. This is thus further proof that the electronic structure of SWNTs is extensively perturbed by sidewall oxidation. This evident disruption of the extended π system in SWNTs is consistent with sidewall functionalization and moreover, is not observed on derivatization, localized simply at the end caps. The generally smaller diameters[12,51] (0.7−1.1 nm) of HiPco tubes, as compared with tubes produced by traditional arc discharge or laser vaporization techniques, likely makes them more susceptible to sidewall oxidation than larger tubes.

III. Achieving a Degree of Control over Functional Groups in Ozonized SWNTs. Whereas we have previously demonstrated purification and sidewall functionalization, our next results present a certain degree of control over SWNT chemical derivatization using ozonolysis without disrupting the tubular bundles. In independent runs, the ozonized tubes were reacted with several types of reagents known to cleave the primary ozonide intermediates in different ways (Figure 6). In organic systems, primary ozonides will undergo oxidative cleavage with H_2O_2 to give primarily carboxylic acid and ester groups[52] and with DMS to yield predominantly carbonyl (keto or aldehydic) functionalities.[53,54] Similarly, reductive cleavage with $NaBH_4$ leads to the generation of alcoholic groups.[55,56] High-resolution XPS spectra show that upon ozonolysis followed by cleavage with the reagents described above, the relative concentrations of the oxygenated functionalities do indeed vary from sample to sample. Because of the extensive treatment and hence, high purity of the resultant SWNT samples studied, we believe our XPS data to be sufficiently reliable.

To support this assertion, we observe that no noticeable trace of Na, B, or S was detected in the XPS analysis, indicating that the cleaving reagents were completely removed by the washing process. Regarding the presence of iron[13] due to the metal catalysts in raw HiPco tubes (which is normally 4−5%), treatment with O_3, followed by the appropriate chemical workup, was found to lower the Fe content to 1.47% (**Ctrl** sample). After

TABLE 1: Relative Percentages of Surface-Functional, Oxygenated Groups Obtained from Curve Fitting of the C_{1s} Peaks of the SWNT HiPco Samples Subjected to Ozonolysis in Methanol at −78 °C, Followed by Selective Chemical Treatments

sample	C−O species (alcohol)	C═O species (aldehyde/ketone)	O−C═O species (carboxylic acid/ester)
Ctrl (untreated)	13.3	50.8	35.9
1 (reaction with H_2O_2)	37.0	9.4	53.6
2 (reaction with DMS)	28.7	41.1	30.2
3 (reaction with $NaBH_4$)	29.1	36.3	34.6

one cycle of $NaBH_4$ addition followed by HCl washes, following ozonolysis, the Fe content in sample **3** was reduced to 0.48%. Notably, the amount of Fe in sample **1**, from a combined ozonolysis/hydrogen peroxide treatment, was found to be the lowest at 0.25%. Use of H_2O_2 alone on raw tubes can only reduce the Fe content only to 1.37% whereas utilization of $NaBH_4$/HCl alone will lower Fe content to only 1.16%.

The distribution of functionalities has been deduced from the high-resolution C_{1s} XPS spectra (Figure 7). The data can be fitted to values close to those for graphite and more specifically, to those reported in the literature for carbon nanotubes.[15,57,58] Figure 7 shows the high-resolution C_{1s} spectra of the various functionalized nanotubes. In each spectrum, the main peak at 284.6 eV is assigned to the C_{1s} binding energy for the SWNTs, representing the elemental sp^2 and sp^3 carbon atom; it has the same shape as the C_{1s} peak in graphite. The shoulder of the main peak is composed of three peaks, assigned to the C_{1s} of hydroxyl carbon (286.3 eV), that of carbonyl carbon (287.6 eV), and ultimately, that of carboxyl carbon (288.8 eV). The higher binding energies correlate with the increased numbers of O atoms bonded to C since the electronegative O atoms induce a positive charge on a carbon atom.[58] Small features[24] at the high binding energy side at ∼290.7 eV have been relegated to the $\pi-\pi^*$ transitions accompanying the C_{1s} excitation and are not included in the quantifications of the oxygenated functionalities.

Table 1 summarizes the relevant results. On simply passing ozone through a solution of nanotubes without the presence of a "cleaving" agent (**Ctrl** sample), the carboxyl and carbonyl species are found to predominate. This observation is consistent with gaseous ozonolysis data where quinone and ester species were found to be the most prevalent species.[28] The increased alcohol content, noted in solution as compared to gaseous ozonolysis, is expected to arise from spontaneous decomposition of the ozonide intermediate in methanol.

On cleaving the ozonide with H_2O_2, namely sample **1**, the carboxylic acid/ester species become the major functional groups. Oxidative cleavage with DMS, in sample **2**, ensures that the keto or aldehydic groups are the most abundant functionality. Finally, upon reductive cleavage of the ozonide intermediate through $NaBH_4$ reduction, yielding sample **3**, the amount of alcoholic and ether species is more than double what one might expect with the untreated **Ctrl** sample. It is of note that most of the ether functionalities, if formed on the SWNT surface, would be transformed to alcohol because of the choice of methanol as the solvent.

It should be stressed that the protocol described, at the moment, cannot generate 100% abundance of a particular oxygenated functional group. One of the main reasons for not obtaining such favorable selectivity is that the unstable ozonide intermediate may rapidly quench[59] (especially in solution), form high yields of secondary ozonides, or even react with any remaining contaminants, such as Fe impurities. All of these secondary processes provide for competing pathways and hence, lead to different product distributions from the full conversion values expected. Indeed, though some degree of chemical control nevertheless is possible, the lingering presence of catalytic iron means that absolute control is very difficult to obtain. H_2O_2 treatment, after ozonolysis, yields greater than 50% carboxylic acid (−COOH) functionalities, the predominant group in that set of data. These results are a clear improvement over conventional nanotube processing procedures, such as Ar^+ ion sputtering,[57] where the percentage of carboxylic groups is ∼15%. The large alcohol content in this sample, though, likely arises from a H_2O_2−iron particle interaction, which can form reactive secondary hydroxyl radicals. The importance of cleavage of the ozonide intermediate in generating the high quantity of carboxylic acid moieties also becomes apparent as treatment of HiPco tubes with simply hydrogen peroxide, without ozonolysis, yields predominantly hydroxyl groups (47%) and a noticeably lower amount of carboxylic acid groups (22%).

While generating other oxygenated functional groups solely by ozonide cleavage is rather difficult and while not all of the major issues are fully resolved, our data provide for a promising and rational strategy and foundation with which to approach this very challenging problem of controlling functional group distributions on nanotube surfaces. For instance, it is evident that $NaBH_4$ was the most appropriate and logical reagent for generating almost 30% of alcoholic species, comparable to the best results obtained by thermal treatment in air and ion sputtering.[57,60] Similarly, use of DMS led to a reasonable yield of over 40% of keto and aldehyde groups, the highest among all of the workup reagents tried. With ion processing,[57] the analogous keto/aldehyde yield is ∼25%.

Conclusions

Rational functionalization of the sidewalls of SWNTs has been accomplished by a relatively facile ozonolysis process in solution. The methodology not only conserves the structural integrity of the tube bundles but also purifies them, removing a large number of metal impurities and amorphous carbon entities.

Significantly, this work bears out the theoretical prediction that 1,3-dipolar cycloaddition to the SWNT sidewalls is experimentally achievable. In fact, these experiments indicate that a certain degree of control over the presence of particular functional groups on the surfaces of these SWNTs can be obtained by judicious choice of the appropriate cleaving agent, all of which can be achieved with minimal sample loss. More importantly, this protocol presents a nondestructive, low-temperature method of introducing oxygenated functionalities directly onto the sidewalls and not simply at the end caps of SWNTs. Thus, molecular species, that can be currently tethered to the ends of the nanotubes, can now be chemically dispersed along the sidewalls as well, with implications for the design of nanotube-based optoelectronic devices.

Further efforts will be targeted at optimizing the ozonolysis process to gain further selectivity in terms of functional group distributions. Interactions of multiwalled nanotubes with O_3 will also be the focus of future work.

Acknowledgment. We acknowledge support of this work through startup funds provided by the State University of New York at Stony Brook as well as Brookhaven National Laboratory. Acknowledgment is also made to the donors of the Petroleum Research Fund, administered by the American Chemical Society, for support of this research. Sigma Xi is also

acknowledged for a Grant-in-Aid of Research.We also thank Dr. James Quinn for his guidance with the SEM/TEM work and Pankaj D. Rege for helpful discussions. The assistance of Dana Kelley and Tom Tague (Brüker Optics), with near-IR and Raman analyses, has been appreciated. Drew Hirt (Materials Research Laboratories, Inc.) is acknowledged for his work with the XPS results.

References and Notes

(1) Dresselhaus, M. S.; Dresselhaus, G.; Eklund, P. C. *Science of Fullerenes and Carbon Nanotubes*; Academic Press: New York, 1996.
(2) Falvo, M. R.; Clary, G. J.; Taylor, R. M. I.; Chi, V.; Brooks, F. P. J.; Washburn, S.; Superfine, R. *Nature* **1997**, *389*, 582.
(3) Odom, T. W.; Huang, J.-L.; Kim, P.; Lieber, C. M. *Nature* **1998**, *391*, 62.
(4) Chen, Y. K.; Green, M. L. H.; Griffin, J. L.; Hammer, J.; Lago, R. M.; Tsang, S. C. *Adv. Mater.* **1996**, *8*, 1012.
(5) Huang, S.; Dai, L. *J. Phys. Chem. B*, **2002**, *106*, 3543.
(6) Niyogi, S.; Hu, H.; Hamon, M. A.; Bhowmik, P.; Zhao, B.; Rozenhak, S. M.; Chen, J.; Itkis, M. E.; Meier, M. S.; Haddon, R. C. *J. Am. Chem. Soc.* **2001**, *123*, 733.
(7) Zhao, B.; Hu, H.; Niyogi, S.; Itkis, M. E.; Hamon, M. A.; Bhowmik, P.; Meir, M. S.; Haddon, R. C. *J. Am. Chem. Soc.* **2001**, *123*, 11673.
(8) Abatemarco, T.; Stickel, J.; Belfort, J.; Frank, B. P.; Ajayan, P. M.; Belfort, G. *J. Phys. Chem. B* **1999**, *103*, 3534.
(9) Bonard, J.-M.; Stora, T.; Salvetat, J.-P.; Maier, F.; Stockli, T.; Duschl, C.; Forro, L.; de Heer, W. A.; Chatelain, A. *Adv. Mater.* **1997**, *9*, 827.
(10) Chiang, I. W.; Brinson, B. E.; Smalley, R. E.; Margrave, J. L.; Hauge, R. H. *J. Phys. Chem. B* **2001**, *105*, 1157.
(11) Hernadi, K.; Siska, A.; Thien-Nga, L.; Forro, L.; Kiricsi, I. *Solid State Ionics* **2001**, *141*, 203.
(12) Rinzler, A. G.; Liu, J.; Dai, H.; Nikolaev, P.; Huffman, C. B.; Rodriguez-Macias, F. J.; Boul, P. J.; Lu, A. H.; Heymann, D.; Colbert, D. T.; Lee, R. S.; Fischer, J. E.; Rao, A. M.; Eklund, P. C.; Smalley, R. E. *Appl. Phys. A: Mater. Sci. Process.* **1998**, *67*, 29.
(13) Chiang, I. W.; Brinson, B. E.; Huang, A. Y.; Willis, P. A.; Bronikowski, M. J.; Margrave, J. L.; Smalley, R. E.; Hauge, R. H. *J. Phys. Chem. B* **2001**, *105*, 8297.
(14) Bond, A. M.; Miao, W.; Raston, C. *Langmuir* **2000**, *16*, 6004.
(15) Hiura, H.; Ebbesen, T. W.; Tanigaki, K. *Adv. Mater.* **1995**, *7*, 275.
(16) Chen, J.; Rao, A. M.; Lyuksyutov, S.; Itkis, M. E.; Hamon, M. A.; Hu, H.; Cohn, R. W.; Eklund, P. C.; Colbert, D. T.; Smalley, R. E.; Haddon, R. C. *J. Phys. Chem. B.* **2001**, *105*, 2525.
(17) Riggs, J. E.; Guo, Z.; Carroll, D. L.; Sun, Y.-P. *J. Am. Chem. Soc.* **2000**, *122*, 5879.
(18) Banerjee, S.; Wong, S. S. *Nano Lett.* **2002**, *2*, 49.
(19) Banerjee, S.; Wong, S. S. *J. Am. Chem. Soc.* **2002**, *124*, 8940.
(20) Banerjee, S.; Wong, S. S. *Nano Lett.* **2002**, *2*, 195.
(21) Shimoda, H.; Gao, B.; Tang, C. P.; Kleinhammes, A.; Fleming, L.; Wu, Y.; Zhou, O. *Phys. Rev. Lett.* **2002**, *88*, 15502.
(22) Liu, C.; Fan, Y. Y.; Liu, M.; Cong, H. T.; Cheng, H. M.; Dresselhaus, M. S. *Science* **1999**, *286*, 1127.
(23) Bandosz, T.; Jagiello, J.; Schwarz, J. A. *Langmuir* **1993**, *9*, 2518.
(24) Kuznetsova, A.; Yates, J. T., Jr.; Liu, J.; Smalley, R. E. *J. Chem. Phys.* **2000**, *112*, 9590.
(25) Lu, X.; Zhang, L.; Xu, X.; Wang, N.; Zhang, Q. *J. Phys. Chem. B* **2002**, *106*, 2136.
(26) Deng, J.-P.; Mou, C.-Y.; Han, C.-C. *Fullerene Sci. Technol.* **1997**, *5*, 1033.
(27) Heymann, D.; Bachilo, S. M.; Weisman, R. B.; Cataldo, F.; Fokkens, R. H.; Nibbering, N. M. M.; Vis, R. D.; Chibante, L. P. F. *J. Am. Chem. Soc.* **2000**, *122*, 11473.
(28) Mawhinney, D. B.; Naumenko, V.; Kuznetsova, A.; Yates, J. T., Jr.; Liu, J.; Smalley, R. E. *J. Am. Chem. Soc.* **2000**, *122*, 2383.
(29) Nikolaev, P.; Bronikowski, M. J.; Bradley, R. K.; Rohmund, F.; Colbert, D. T.; Smith, K. A.; Smalley, R. E. *Chem. Phys. Lett.* **1999**, *313*, 91.
(30) Ajayan, P. M.; Ebbesen, T. W.; Ichihashi, T.; Iijima, S.; Tanigaki, K.; Hiura, H. *Nature (London)* **1993**, *361*, 333.
(31) Ebbesen, T. W.; Ajayan, P. M.; Hiura, H.; Tanigaki, K. *Nature (London)* **1994**, *367*, 519.
(32) Srivastava, D.; Brenner, D. W.; Schall, J. D.; Ausman, K. D.; Yu, M.; Ruoff, R. S. *J. Phys. Chem. B* **1999**, *103*, 4330.
(33) Wang, Y.; Zhang, O.; Shishido, T.; Takehira, K. *J. Catal.* **2002**, *209*, 186.
(34) Kukovecz, A.; Kramberger, C.; Holzinger, M.; Kuzmany, H.; Schalko, J.; Mannsberger, M.; Hirsch, A. *J. Phys. Chem. B* **2002**, *106*, 6374.
(35) Yu, Z.; Brus, L. E. *J. Phys. Chem. B* **2001**, *105*, 1123.
(36) Yu, Z.; Brus, L. E. *J. Phys. Chem. B* **2001**, *105*, 6831.
(37) Rao, A. M.; Richter, E.; Bandow, S.; Chase, B.; Eklund, P. C.; Williams, K. A.; Fang, S.; Subbaswamy, K. R.; Menon, M.; Thess, A.; Smalley, R. E.; Dresselhaus, G.; Dresselhaus, M. S. *Science* **1997**, *275*, 187.
(38) Corio, P.; Brown, S. D. M.; Marucci, A.; Pimenta, M. A.; Kneipp, K.; Dresselhaus, G.; Dresselhaus, M. S. *Phys. Rev. B* **2000**, *61*, 13202.
(39) Bahr, J. L.; Yang, J.; Kosynkin, D. V.; Broniskowski, M. J.; Smalley, R. E.; Tour, J. M. *J. Am. Chem. Soc.* **2001**, *123*, 6536.
(40) Brown, S. D. M.; Corio, P.; Marucci, A.; Pimenta, M. A.; Dresselhaus, M. S.; Dresselhaus, G. *Phys. Rev. B* **2000**, *61*, 7734.
(41) Dresselhaus, M. S.; Dresselhaus, G.; Jorio, A.; Souza Filho, A. G.; Saito, R. *Carbon* **2002**, *40*, 2043.
(42) Alvarez, L.; Righi, A.; Guillard, T.; Rols, S.; Anglaret, E.; Laplaze, D.; Sauvignol, J.-L. *Chem. Phys. Lett.* **2000**, *316*, 186.
(43) Kataura, H.; Kumazawa, Y.; Mainwa, Y.; Umezu, I.; Ohtsuka, Y.; Achiba, Y. *Synth. Met.* **1999**, *103*, 2555.
(44) Bahr, J. L.; Tour, J. M. *Chem. Mater.* **2001**, *13*, 3823.
(45) Georgakilas, V.; Kordatos, K.; Prato, M.; Guldi, D. M.; Holzinger, M.; Hirsch, A. *J. Am. Chem. Soc.* **2002**, *124*, 760.
(46) Boul, P. J.; Liu, J.; Mickelson, E. T.; Huffman, C. B.; Ericson, L. M.; Chiang, I. W.; Smith, K. A.; Colbert, D. T.; Margrave, J. L.; Smalley, R. E. *Chem. Phys. Lett.* **1999**, *310*, 367.
(47) Liu, J.; Rinzler, A. G.; Dai, H.; Hafner, J. H.; Bradley, R. K.; Boul, P. J.; Lu, A.; Iverson, T.; Shelimov, K.; Huffman, C. B.; Rodriguez-Macias, F.; Shon, Y. S.; Lee, T. R.; Colbert, D. T.; Smalley, R. E. *Science* **1998**, *280*, 1253.
(48) Marcoux, P. R.; Schreiber, J.; Batail, P.; Lefrant, S.; Renouard, J.; Jacob, G.; Albertini, D.; Mevellec, J.-V. *Phys. Chem. Chem. Phys.* **2002**, *4*, 2278.
(49) Chen, J.; Hamon, M. A.; Hu, H.; Chen, Y.; Rao, A. M.; Eklund, P. C.; Haddon, R. C. *Science* **1998**, *282*, 95.
(50) Hamon, M. A.; Itkis, M. E.; Niyogi, S.; Alvaraez, T.; Kuper, C.; Menon, M.; Haddon, R. C. *J. Am. Chem. Soc.* **2001**, *123*, 11292.
(51) Ichida, M.; Mizuno, S.; Tani, Y.; Saito, Y.; Nakamura, A. *J. Phys. Soc. Jpn.* **1999**, *68*, 3131.
(52) Pasero, J.; Chouteau, J.; Naudet, M. *Bull. Soc. Chim. Fr.* **1960**, 1717.
(53) Appell, R. B.; Tomlinson, I. A.; Hill, I. *Synth. Commun.* **1995**, *25*, 3589.
(54) Hon, Y. S.; Lin, S. W.; Chen, Y. J. *Synth. Commun.* **1993**, *23*, 1543.
(55) Lautens, M.; Abd-El-Aziz; Alaa, S.; Lough, A. *J. Org. Chem.* **1990**, *55*, 5305.
(56) Moore, W. R.; Ozretich, T. M. *Tetrahedron Lett.* **1967**, *33*, 3205.
(57) Lee, W. H.; Kim, S. J.; Lee, W. J.; Lee, J. G.; Haddon, R. C.; Reucroft, P. J. *Appl. Surf. Sci.* **2001**, *181*, 121.
(58) Ago, H.; Kugler, T.; Cacialli, F.; Salaneck, W. R.; Shaffer, M. S. P.; Windle, A. H.; Friend, R. H. *J. Phys. Chem. B* **1999**, *103*, 8116.
(59) Harding, L. B.; Goddard, W. A., III. *J. Am. Chem. Soc.* **1978**, *100*, 7180.
(60) Sano, M.; Kamino, A.; Shinkai, S. *Proceedings of the 3rd International Nanotube Symposium*, Boston, MA, July 5−12, 2002. http://dielc.kaist.ac.kr/nt02/abstracts/P160.shtml.